JOURNAL OF MATERIALS SCIENCE 31 (1996) 2379–2384

Influence of *R*-curve behaviour on strength degradation due to Hertzian indentation

S. WIDJAJA, J. E. RITTER*, K. JAKUS
Department of Mechanical Engineering, University of Massachusetts, Amherst, MA 01003, USA

The influence of *R*-curve behaviour on the post-indentation strength of two types of alumina was studied using Hertzian indentation. Soda–lime glass was included in the study to represent a material which does not exhibit *R*-curve behaviour. Specimens were indented with a spherical indentor with increasing loads. Post-indentation strength was measured in a mineral-oil environment using a ring-on-ring biaxial fixture. Indentation of the two aluminas produced the typical Hertzian crack pattern with a somewhat greater statistical variability than that found in soda–lime glass. The strength of the two aluminas fell into four different regimes that were separated by the onset of ring, cone, and radial crack formation, respectively. *R*-curve behaviour did not appreciably influence the results, undoubtedly due to the relatively narrow range of indentation loads where failure was controlled by ring and cone cracks. These strength results contrast to those obtained for soda–lime glass. In soda–lime glass, ring and cone crack nucleation occurred simultaneously with a sudden drop in strength followed by a gradual decline in strength with increasing indentation load, in accordance with the prediction of Hertzian cone-crack theory.

1. Introduction

Strength degradation of ceramic components is often caused by in-service damage due to localized contact loads or particle impact. It is generally believed that impact damage can be modelled by the idealized crack systems produced by sharp (Vickers) and blunt (Hertzian) indentors [1]. Sharp indentation produces two distinctive crack systems: radial cracks that are responsible for strength degradation and lateral cracks that are the source of material removal. Both of these crack systems are driven to their equilibrium size by the residual stress that forms about the indentation due to the mismatch between the plastic zone underneath the indentor and the surrounding elastic matrix. Blunt indentation produces elastic deformation below the indentor that results in a ring/cone-crack combination.

Radial cracks can be modelled to a good approximation by a half-penny crack with a constant residual force located at the centre of the surface trace of the crack [2, 3]. This model, with the use of a material-independent calibrated constant, predicts the extent of strength degradation in terms of indentation load and substrate material properties (fracture toughness, elastic modulus and hardness). In ceramics that exhibit crack length-dependent toughness, i.e. *R*-curve behaviour, Vickers indentation causes less severe strength degradation than would be expected for constant toughness. Fig. 1 shows our previous Vickers indentation strength degradation for AD995 [4]. Without

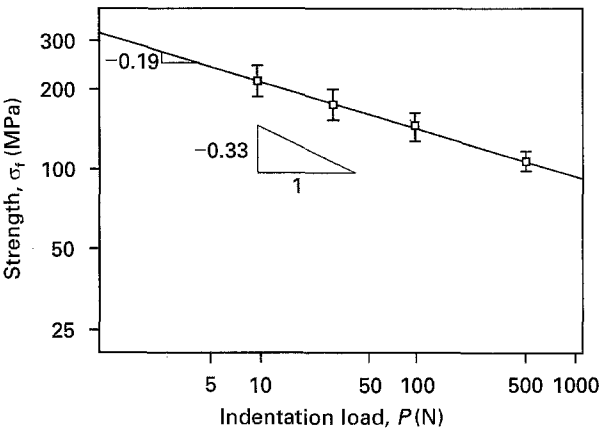

Figure 1 Post-Vickers indentation strength of AD995 alumina plotted as a function of indentation load.

R-curve behaviour, the slope in Fig. 1 should have been $-1/3$. On the other hand, the Hertzian cone-crack is a relatively complex three-dimensional crack, and no simple model for strength degradation, analogous to the radial crack model, has been developed [5–8]. The influence of *R*-curve behaviour on the Hertzian cone-crack and the resulting strength degradation has not been studied, except for some initial results by the present authors [9].

The objective of this research was to study the effect of *R*-curve behaviour on strength degradation due to Hertzian indentation. For this purpose, the Hertzian

*Author to whom all correspondence should be addressed.

0022–2461

TABLE I Properties of the studied materials

Material	Nominal grain size (μm)	Purity (%)	Density ($kg\,m^{-3}$)	Elastic modulus	Hardness (GPa)	Poisson's ratio
Soda–lime glass	–	–	2460	70	5.5	0.23
AD90[a]	4	90.0	3600	276	11.3	0.22
AD995[a]	17	99.5	3890	372	14.2	0.22

[a] Coors Porcelain, Golden, CO.

strength degradation of two aluminas and soda–lime glass was determined. Vickers indentation tests have shown that one of the aluminas exhibits strong room-temperature R-curve behaviour and the other alumina weak R-curve behaviour; soda–lime glass does not show any R-curve behaviour.

2. Experimental procedure

The materials that were studied in this research were two types of sintered alumina and soda–lime glass. The material specifications are summarized in Table I. The alumina specimens were received in the form of discs with a diameter of 40 mm and a thickness of 2 mm. The specimens were polished on one side by the manufacturer to a surface finish of 12.7 μm. Soda–lime glass specimens were cut from 3 mm window glass sheets into approximate dimensions of 58 mm × 58 mm, and were annealed at 520 °C for 1 h and slowly cooled to relieve any residual stresses. Prior to indentation and strength testing, all specimens were randomized to avoid any systematic error.

Indents were placed in the centre of tensile surface of the specimen using a 4.76 mm steel sphere for soda–lime glass and a 4 mm diameter WC–6% Co sphere (Industrial Tectronics, Ann Arbor, MI) for the aluminas. Indentation was performed on a Universal Testing Machine (Model 6025, Instron Corp., Canton, MA) with loading and unloading rates of $0.01\,cm\,min^{-1}$. The maximum indentation load was held for 20 s before unloading, and it ranged from 300–2500 N for alumina specimens and from 100–1500 N for soda–lime glass.

To measure the radius of the ring cracks, a few specimens were coated with gold using a commercial SEM coating apparatus before indentation. This coating technique caused the ring cracks to be easily observed under an optical microscope (Olympus AHBT). To measure the radius of the cone base, the specimens were cut using a diamond-wheel and then polished. The cone-crack length, the cone-base radius and the angle between the cone-crack and the specimen's surface, were measured with an optical microscope.

The strength of the indented specimens was determined at room temperature using a ring-on-ring biaxial fixture. The support and the loading rings of the test fixture had diameters of 28.6 mm and 9.2 mm, respectively. Prior to strength testing, the indentation site was covered with mineral oil to minimize subcritical crack growth during the test. All fracture tests were done on a Universal Testing Machine (Model 6025, Instron Corp., Canton, MA) at a crosshead rate of $5\,mm\,min^{-1}$, corresponding to a stressing rate of about $200\,MPa\,s^{-1}$. The equation to calculate fracture strength from fracture load is given by Shetty *et al.* [10]. Approximately six specimens per indentation load were tested.

Strength degradation of the same materials due to Vickers indentation was previously measured using an indentation load range of 5–500 N [4, 11], as shown in Fig. 1 for AD995. These indentation loads produced radial crack lengths in the range of 25–520 μm. The crack length-dependent toughness (R-curve behaviour) calculated from the Vickers indentation strength results of the two aluminas were fitted to the equation [12]

$$K_C(c) = k\,c^m \quad (1)$$

where $K_C(c)$ is fracture toughness ($MPa\,m^{1/2}$), c is the crack length (m), and k and m are constants depending on the material tested. For AD90 and AD995 aluminas, m was found to be 0.05 and 0.18, respectively, as determined from Vickers indentation [4]. The parameter must be between 0 and 0.5 [12]. If $m = 0$, then $K_C(c)$ is independent of crack length and is equal to the fracture toughness, K_C. Equation 1 will be used in the evaluation of the Hertzian indentation strength results.

3. Results and discussion

3.1. Sequence of cracking

Upon Hertzian indentation, both AD aluminas and soda–lime glass exhibited similar crack patterns. A schematic representation of Hertzian indentation and the corresponding crack pattern is shown in Fig. 2. Predominant features of this crack pattern are a series of ring cracks surrounding the contact area and a cone-crack emanating from one of the ring cracks. For all materials it was observed that at relatively low indentation loads only partial ring cracks formed. As the indentation load was increased, these partial ring cracks grew into fully developed ones, and eventually a collection of several concentric cracks appeared around the contact zone. Ring crack formation was probabilistic in nature, such that a given indentation load did not always produce a ring crack. The probability of producing ring cracks as a function of indentation load for the AD aluminas is shown in Fig. 3. The probability was calculated from the ratio of the indents that produced a partially or fully developed ring crack and the total number of

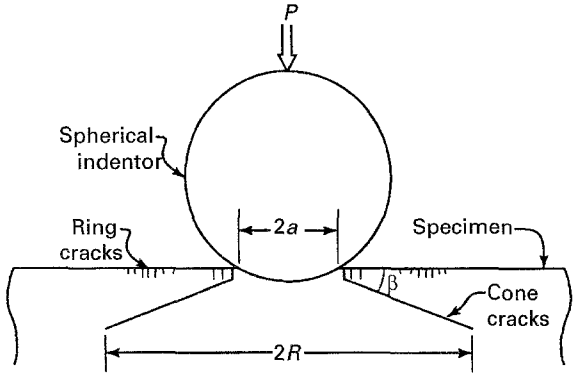

Figure 2 The Hertzian crack system.

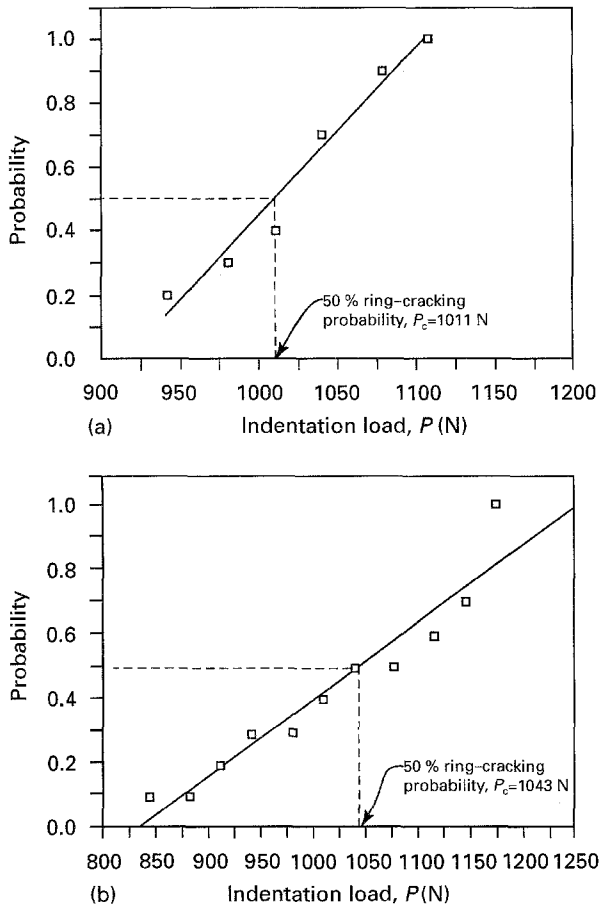

Figure 3 Ring-cracking probability plotted as a function of indentation load for (a) AD90 alumina and (b) AD995 alumina. (□) Data, (—) regression line.

indentations (typically 10) at a given load. The load at 50% probability was defined as the critical load for ring crack formation, P_c [13]. These critical loads for ring crack formation are given in Table II.

At indentation loads above the ring crack formation, a cone-crack nucleated from one of the ring cracks in soda–lime glass and AD90 alumina. The measured cone-crack angle, β, for soda–lime glass and AD90 alumina was 22° and 24°, respectively. Similar to ring cracking, cone cracking was also probabilistic in nature. The critical load for 50% probability of cone cracking was determined and is given in Table II. Unfortunately, due to the opacity of AD995 alumina, it was not possible to observe the subsurface cone-

TABLE II Critical loads for crack formation

	Critical load (N)		
	Soda–lime glass	AD90	AD995
Ring crack	295	1010	1045
Cone crack	410	1375	1250
Radial crack	–	1865	2050

[a] Estimated from strength data.

cracks and these cone-cracks were not discernible in the fracture surfaces after strength testing. Therefore, for AD995 cone-crack nucleation was inferred from the break in slope of the strength curve, as will be discussed below.

With further increase in indentation loads, radial cracks, emanating from the ring cracks, were observed in the alumina specimens. At a given indent, these radial cracks varied in number from four to six and were evenly spaced, by-and-large, about the indent. It was observed that some of the radial cracks were diagonally opposite across the contact area. However, not all of the radial cracks appeared in diagonal pairs. Again, radial cracking was probabilitistic in nature and the critical load for 50% probability of radial cracking was determined and is given in Table II. The contact pressure, defined as $P/\pi a^2$, at the onset of radial cracking can be estimated from the Hertzian relationship for the contact radius [7]

$$a^3 = \frac{4k P_r}{3E_1} \tag{2}$$

where E_1 is the elastic modulus of the specimen, r is the indentor radius and

$$k = \frac{9}{16}\left[(1-\nu_1^2) + (1-\nu_2^2)\frac{E_1}{E_2}\right] \tag{3}$$

where ν_1 and ν_2 are Poisson's ratio of the specimen and the indentor, respectively, and E_2 is the elastic modulus of the indentor. Taking $\nu_2 = 0.22$ and $E_2 = 641$ GPa, the contact pressure at the onset of radial cracking was calculated to be 10.4 GPa for AD90 and 12.2 GPa for AD995. From Table I it can be seen that this estimated contact pressure is about the same as the hardness.

It is of interest to compare the fracture toughness derived from Vickers radial cracking to Hertzian cone cracking. By modelling the radial crack as a half-penny crack with a constant force load at its centre, Anstis *et al.* [2] derived the following relationship for materials with constant toughness

$$\frac{P}{c^{3/2}} = \frac{1}{\xi}\left(\frac{H}{E}\right)^{1/2} K_C \tag{4}$$

where P is indentation load, c is the radial crack size, H is hardness, E is elastic modulus and ξ is a dimensionless constant that was calibrated over a wide range of ceramics to be 0.016 [2]. By substituting $K_C(c)$ from Equation 1 into Equation 4 for K_C, it can be shown that the radial crack size is relatively insensitive to m [12]. That is, crack-size measurements are

TABLE III Crack sizes and the corresponding fracture toughnesses obtained by Vickers and Hertzian indentations

Material	Vickers indentation		Hertzian indentation	
	$\frac{P}{c^{3/2}}$	K_C (MPa m$^{1/2}$)	$\frac{P}{R^{3/2}}$	K_C (MPa m$^{1/2}$)
Soda–lime glass	12.0	0.70	23.5	0.67
AD90 alumina	31.0	2.51	103.8	2.96
AD995 alumina	38.5	3.10	–	–

insensitive to R-curve behaviour. Therefore, by knowing H and E, the fracture toughness, K_C, can be determined from indentation load–radial crack-size data. Table III summarizes radial crack-size data for soda–lime glass [11] and the two aluminas, AD90 and AD995 [4].

Although no simple analysis exists for the Hertzian cone-crack, dimensional analysis indicates that for well-developed cone cracks [5, 6]

$$\frac{P}{R^{3/2}} = \alpha(\nu, \beta)\, K_C \tag{5}$$

where R is the radius of the cone base and $\alpha(\nu, \beta)$ is a dimensionless constant dependent upon Poisson's ratio, ν, and the cone-crack angle, β. Recent finite element analysis [14] indicates that $\alpha = 35.11$ for $\nu = 0.23$ and $\beta = 22°$. Thus, from the measured Hertzian cone-crack parameters for soda–lime glass ($\nu = 0.23$ and $\beta = 22°$) and AD90 ($\nu = 0.22$ and $\beta = 24°$), K_C was calculated from Equation 5 and compared to the values of K_C determined by Vickers indentation, as shown in Table III. The excellent agreement is evident and gives support to the use of Equation 5, coupled with finite element analysis, in determining fracture toughness from Hertzian cone-crack data.

3.2. Strength degradation

Strength degradation due to a Hertzian cone-crack would be expected to be related to the cone-base radius, R, multiplied by an appropriate flaw-shape parameter [6]. Thus, post-Hertzian indentation strength for a constant toughness is

$$\sigma_f = \frac{K_C}{[\pi\Omega(\beta) R]^{1/2}} \tag{6}$$

where $\Omega(\beta)$ is a dimensionless constant dependent upon the cone-crack angle, β. Substituting Equation 5 into Equation 6 and taking $\alpha = 35.11$ gives

$$\sigma_f = \frac{(35.11)^{1/3} K_C^{4/3}}{[\pi\Omega(\beta)]^{1/2}} P^{-1/3} \tag{7}$$

Lawn *et al.* [6] estimated that $\Omega(\beta = 22°) = 0.25$ and $\Omega(\beta = 24°) = 0.30$ based on an approximate two-dimensional analysis.

Fig. 4 shows the post-Hertzian indentation strength of soda-lime glass as a function of indentation load.

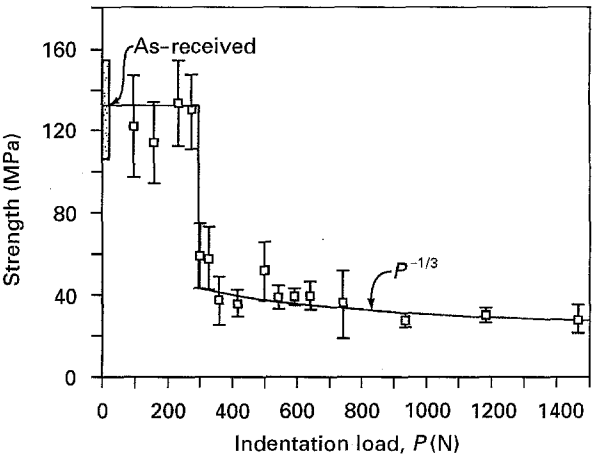

Figure 4 Post-Hertzian indentation strength of soda–lime glass plotted as a function of indentation load.

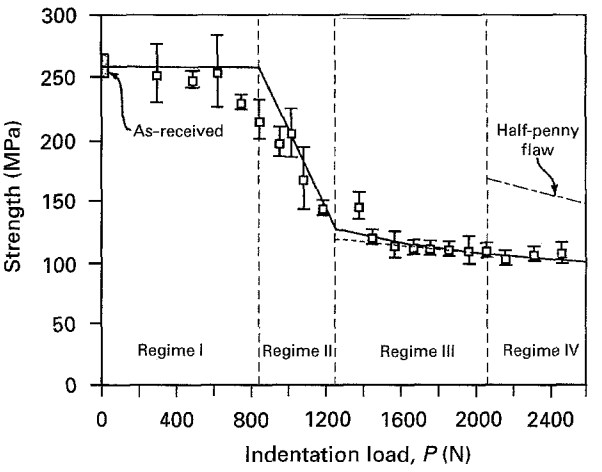

Figure 5 Post-Hertzian indentation strength of AD995 alumina plotted as a function of indentation load. (———) Predicted strength based on a half-penny crack. (—) $P^{-1/3}$, (– – –) $P^{(2m-1)/(2m+3)}$ with $m = 0.18$.

As seen from the figure, the strength was essentially unaffected by indentation load until ring/cone cracks started to form. The onset of cracking caused a precipitious decrease in strength. Further increases in load caused a steady, but slow decrease in strength. Equation 7 was regressed to the data in this regime. It can be seen that Equation 7 fits the data well, and Ω determined from the regression analysis was 0.11 for $K_C = 0.67$ MPa m$^{1/2}$. This value of Ω does not agree with the estimate of 0.25 by Lawn *et al.* [6]. Thus, it is believed that a more exact stress intensity analysis for the three-dimensional Hertzian cone-crack is needed. In the interim, Ω must be viewed as a material constant that can be determined from calibration tests of strength as a function of indentation load. Without finite element analysis, the material-dependent calibrated constant becomes α/Ω.

Fig. 5 shows the post-Hertzian indentation strength of AD995 alumina as a function of indentation load. As shown on the figure, the strength behaviour can be divided into four regimes.

Regime I: in this regime no crack formation was observed and strength was essentially unaffected by

indentation. Within experimental scatter, the strength was equal to the previously determined as-received strength (265 ± 6) MPa, shown by a horizontal line on the figure. The boundaries of this regime extend from zero indentation load to 830 N which represents the onset of ring crack formation (Fig. 3).

Regime II: in this regime the strength showed a monotonic decrease from 265 MPa to 125 MPa that corresponds to the progressive increase of ring-crack formation. This regime extends from essentially 0%–100% ring-crack formation, corresponding to 830–1250 N, respectively. The solid line through the data points was drawn to illustrate the decreasing trend in strength.

Regime III: at approximately an indentation load of 1250 N, the slope of the strength showed a sudden change. Although strength continues to decrease with increasing indentation load, it does so at a noticeably lesser extent. This regime extends from the break in slope, i.e. 100% ring-crack formation, to the indentation load of 2050 N, where radial cracks were observed on the specimen's surface. It is believed that regime III represents where cone-cracks become the strength-controlling flaw. Therefore, Equation 7 was best-fit to the data in this regime by regressing only the last seven data points of this regime because the first point was deemed to be an outlier. The solid line drawn through the data in this regime is the best-fit line representing Equation 7 and the good agreement is evident, showing that strength to good approximation falls off as $P^{-1/3}$. Also, the good-fit of cone-crack strength equation to the data in regime III gives convincing evidence that cone cracks are the strength-controlling flaws in regime III. Taking $\alpha = 35.11$ and $K_C = 3.10\ \text{MPa m}^{1/2}$, Ω determined from the regression analysis was 0.34.

Equation 7 can be extended to include R-curve effects by substituting Equation 1 into Equation 7 and using Equation 5 to give

$$\sigma_f = \frac{1}{[\pi\Omega(\beta)]^{1/2}} (35.11)^{(1-2m)/(3+2m)} k^{4/(3+2m)} P^{(2m-1)/(3+2m)} \quad (8)$$

Equation 8 was regressed to the data in regime III using $m = 0.22$ obtained from Vickers indentation tests on AD995 [4]. This regression line is shown with a dotted line in regime III of Fig. 5. It can be seen that both Equations 7 and 8 fit the data well. The difference in the exponent for the indentation load in the two equations results only in a negligible difference in the strength predictions for the relatively narrow indentation load range of regime III.

Regime IV: this regime represents the indentation load regime where radial cracks were always discernible on the specimen's surface, namely from 2050 N to the maximum indentation load used in this study. It is interesting to note that the rate of strength degradation follows directly that observed in regime III. This implies that cone-cracks continue to dominate strength, rather than the radial cracks. This domination seems reasonable considering that the estimated cone base radius from Equation 5 extends about twice as far as the measured radial cracks. Furthermore, if the radial cracks would dominate, the estimate for strength, assuming the radial cracks are half-penny flaws, is greater than the measured strength. The predicted strength based on a half-penny crack is shown in Fig. 5.

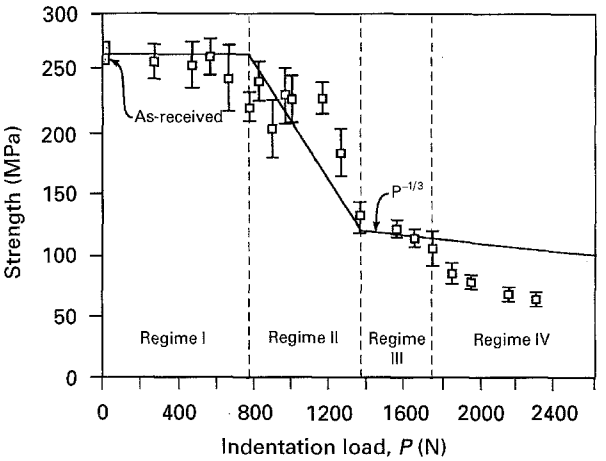

Figure 6 Post-Hertzian indentation strength of AD90 alumina plotted as a function of indentation load.

It is of interest to compare the Hertzian crack formation and the resulting strength degradation in AD995 alumina to that observed in soda–lime glass (Fig. 4). In soda–lime glass, ring and cone crack nucleation seems to occur simultaneously with a sudden drop in strength as contrasted to the observed separation in the onset of ring and cone crack formation in AD995 alumina. Past the onset of cone-crack formation, strength degradation in both soda–lime glass and AD995 alumina follows well the cone-crack strength prediction given by Equation 7.

Fig. 6 shows the post-Hertzian indentation strength of AD90 alumina as a function of indentation load. Similar to AD995 alumina, the strength behaviour of AD90 can be divided into four regimes. In regime I no crack formation was observed and strength was essentially unaffected by indentation. In regime II strength showed a monotonic decrease from about 265–130 MPa, corresponding to the progressive increase in ring crack formation. In regime III, starting at about 1375 N, the slope of the strength curve exhibited a sudden change that corresponded to the observed onset of cone cracking. In this regime, Equation 7 was regressed to the data, giving a value of $\Omega(\beta) = 0.33$ for $K_C = 2.96\ \text{MPa m}^{1/2}$. Using $m = 0.05$ obtained from Vickers indentation tests [4], Equation 8 was also fitted to the data but this regressed line was indistinguishable from Equation 7 as would be expected from the results for AD995 alumina shown in Fig. 5. Regime IV corresponds to where radial cracks were always visible on the specimen's surface. Unlike the results for AD995 alumina, the cone-crack strength prediction of Equation 7 over estimates the strength of AD90 alumina in regime IV. This agrees with the measured radial crack lengths being substantially larger than the measured cone-base radius. Thus, radial cracks are the strength-controlling flaw in regime IV. The different regime IV behaviour between

AD90 and AD995 alumina points to an important R-curve effect, namely the R-value seems to inhibit the formation of a radial crack to a length that is inferior to the cone's dimension in AD995. Interestingly, cone-cracks at a given indentation load must be about the same effective size in the two alumina's because the strengths in regime III are very similar. The question of why the R-curve does not inhibit the formation of the cone-crack remains to be answered.

These post-Hertzian strength results for the two aluminas contrast sharply with strength results due to Vickers indentation. With Vickers indentation, strength is always controlled by radial cracks above a given critical load and the effects of R-curve behaviour can be easily seen. Analysis of radial cracks generated by Vickers indentation indicates that strength depends upon the indentation load in the same way as Hertzian cone-cracks, namely [4]

$$\sigma_f \propto P^{(2m-1)/(2m+3)} \tag{9}$$

However, with Vickers indentation, strength can be measured over a wide range of indentation loads and the influence of R-curve behaviour becomes evident. From Fig. 1 it can be seen that R-curve behaviour causes strength to be less sensitive to indentation load, and regression analysis of these data gives the slope of -0.19, corresponding to $m = 0.18$. In the case of Hertzian indentation, strength of AD995 alumina due to cone-cracks can only be measured over a narrow range of indentation load (1250–2050 N). Thus, the influence of R-curve behaviour is not apparent.

4. Conclusion

R-curve behaviour affects the strength after Hertzian indentation to a much lesser degree than with Vickers indentation. The reason for this can be found in the different crack patterns produced by these two indentation techniques. In Vickers indentation, strength is always dominated by radial cracks, allowing for a broad indentation load range to observe the effects of R-curve. In Hertzian indentation ring- and cone cracks dominated strength in a relatively narrow indentation load range, so that the effects of R-curve behaviour do not become noticeable. Unlike Vickers indentation, post-Hertzian indentation strength due to cone-cracking has to be predicted with the use of a material-dependent calibrated constant.

The implication of these results for the prediction of strength degradation of ceramics resulting from blunt contact damage, is significant. Because the indentation load range over which Hertzian ring- and cone-cracks dominate the strength is relatively small; radial cracking due to elastic/plastic contact controls strength over the range of practical impact loads. Thus, post-impact strength can be predicted for blunt particles based on the previously derived equations for sharp impact [4], except that the calibrated constant must be adjusted to account for the spherical geometry of a projectile [15].

Acknowledgements

This research was supported by National Science Foundation Grant 9012594.

References

1. R. F. COOK and G. M. PHARR, *J. Am. Ceram. Soc.* **73** (1990) 787.
2. G. R. ANSTIS, P. CHANTIKUL, B. R. LAWN and D. B. MARSHALL, *ibid.* **64** (1981) 533.
3. P. CHANTIKUL, G. R. ANSTIS, B. R. LAWN and D. B. MARSHALL, *ibid.* **64** (1981) 539.
4. K. BREDER, J. E. RITTER and K. JAKUS, *ibid.* **71** (1988) 1154.
5. B. R. LAWN and T. R. WILSHAW, *J. Mater. Sci.* **14** (1979) 2001.
6. B. R. LAWN, S. M. WIEDERHORN and H. H. JOHNSON, *J. Am. Ceram. Soc.* **58** (1975) 428.
7. K. ZENG, K. BREDER and D. J. ROWCLIFFE, *Acta Metall. Mater.* **40** (1992) 2595.
8. R. MAUGINOT and D. MAUGIS, *J. Mater. Sci.* **20** (1985) 4354.
9. S. WIDJAJA, K. JAKUS and J. E. RITTER, *Ceram. Eng. Sci. Proc.* (1995) to be published.
10. D. H. SHETTY, A. R. ROSENFELD, P. McGUIRE, B. K. BANSAL and W. H. DUCKWORTH, *Am. Ceram. Soc. Bull.* **59** (1980) 1193.
11. J. E. RITTER, F. M. MAHONEY and K. JAKUS, in "Fracture Mechanics of Ceramics", Vol. 8, edited by R. C. Bradt, A. G. Evans, D. P. H. Hasselman and F. F. Lange (Plenum, New York, 1986) pp. 213–23.
12. R. F. KRAUSE, *J. Am. Ceram. Soc.* **71** (1988) 338.
13. R. WARREN, *Acta Metall.* **26** (1978) 1759.
14. Y. Z. LI and D. A. HILLS, *Trans. ASME J. Appl. Mech.* **58** (1991) 120.
15. D. B. MARSHALL, *J. Am. Ceram. Soc.* **67** (1984) 57.

Received 21 March
and accepted 17 October 1995